JGR Atmospheres

RESEARCH ARTICLE
10.1029/2023JD039167

Investigation of Added Value in Regional Climate Models for East Asian Storm Track Analysis

Ui-Yong Byun[1,2], Eun-Chul Chang[1,2], Joowan Kim[1,2], Joong-Bae Ahn[3], Dong-Hyun Cha[4], Seung-Ki Min[5], and Young-Hwa Byun[6]

[1]Department of Atmospheric Science, Kongju National University, Gongju, Republic of Korea, [2]Earth Environment Research Center, Kongju National University, Gongju, Republic of Korea, [3]Department of Atmospheric Sciences, Pusan National University, Busan, Republic of Korea, [4]Department of Civil, Urban, Earth, and Environmental Engineering, Ulsan National Institute of Science and Technology, Ulsan, Republic of Korea, [5]Division of Environmental Science and Engineering, Pohang University of Science and Technology, Pohang, Republic of Korea, [6]Climate Change Research Team, National Institute of Meteorological Sciences, Jeju, Republic of Korea

Key Points:

- Regional climate models improve accuracy of climate projections for East Asia by simulating local climates at higher resolution than global climate models
- Regional climate models effectively evaluate potential impacts of local climate variability on specific regions and inform local adaptation strategies
- The added value of regional climate models in improving global climate models' bias and agreement with high-resolution reanalysis in mountainous regions is shown

Correspondence to:
E.-C. Chang,
echang@kongju.ac.kr

Citation:
Byun, U.-Y., Chang, E.-C., Kim, J., Ahn, J.-B., Cha, D.-H., Min, S.-K., & Byun, Y.-H. (2023). Investigation of added value in regional climate models for East Asian storm track analysis. *Journal of Geophysical Research: Atmospheres*, *128*, e2023JD039167. https://doi.org/10.1029/2023JD039167

Received 27 APR 2023
Accepted 1 NOV 2023

Author Contributions:
Conceptualization: Eun-Chul Chang
Formal analysis: Joowan Kim
Resources: Joong-Bae Ahn, Dong-Hyun Cha, Seung-Ki Min, Young-Hwa Byun
Writing – original draft: Ui-Yong Byun

Abstract Studies have shown that regional climate models (RCMs) can simulate local climates at a higher resolution for specific regions compared to global climate models (GCMs), making dynamic downscaling using RCMs a more effective approach. Therefore, RCMs have become valuable tools for evaluating the potential impacts of climate change on specific regions and for informing local adaptation strategies. To fully understand the added value (AV) of RCMs, it is essential to understand how the characteristics differ between land and ocean. The complex topography of East Asia, including land and sea, makes it a suitable region for evaluating the AV of RCMs. In this study, we compared two regional simulations that integrated the same RCMs but employed different GCMs from the Coordinated Regional Climate Downscaling Experiment for their ability to simulate storm tracks in East Asia. The results of the RCMs for the period from 1982 to 2005 were compared with their host Coupled Model Intercomparison Project GCM projections and high-resolution reanalysis. In mountainous regions, the AV of the RCMs weakened the bias of the GCM and improved its agreement with the reanalysis due to the dynamical process near the high-resolution topography. In plains and coastal areas, owing to the increase in horizontal resolution and clearly determined coastline in RCMs, small-scale phenomena are well represented, and the storm track of RCMs shows similar values to that of the GCM in maritime regions. This study demonstrates the value of RCMs for improving the accuracy of climate projections in East Asia, informing adaptation strategies, and enhancing climate research.

Plain Language Summary This study looked at how regional climate models can better simulate local climates in specific regions compared to global climate models. By analyzing storm tracks in East Asia, researchers compared regional climate models integrated with different global climate models to better understand the added value of regional climate models. The study found that the regional climate models improved the accuracy of global climate models over mountainous regions and brought them closer to high-resolution reanalysis. In the plains and coastal areas, the regional climate models accurately represented small-scale phenomena due to the increase in horizontal resolution. Overall, this study shows that regional climate models are valuable tools for evaluating climate change in specific regions and can provide more accurate predictions than global climate models alone. This research is essential for improving our understanding of how climate models work and can be used to better predict the future climate of different regions, which can help inform decision-making about mitigating climate change.

1. Introduction

Climate change can lead to numerous socioeconomic problems by shifting climatic conditions within regions. According to Hsiang et al. (2017), the economic loss caused by a 1°C temperature increase reaches up to 1.2% of the total domestic product of the United States. Accurate climate projections and predictions of extreme weather events are essential for minimizing the social and economic losses caused by climate change. To obtain this information, international communities, centered on the Intergovernmental Panel on Climate Change (IPCC), support many scientific activities for climate projection. The Coupled Model Intercomparison Project (CMIP) of the World Climate Research Program (WCRP) is a core project that produces long-term climate projections based on state-of-the-art numerical models from multiple research organizations (Eyring et al., 2016; Meehl et al., 1997;

Taylor et al., 2012). In addition, the recent CMIP (CMIP6; Eyring et al., 2016) provides detailed climate simulations based on various emission scenarios from representative concentration pathways (RCPs; Moss et al., 2010) and shared socioeconomic pathways (SSPs; O'Neill & O'Driscoll, 2015).

Severe weather conditions due to climate change have become more frequent in recent years. Because global climate change scenarios are produced with a relatively coarse-resolution model configuration (approximately 100 km), capturing detailed regional climate characteristics is difficult. Regional climate model (RCMs), which apply a dynamic downscaling technique, have been widely used to determine detailed climatic characteristics that are not well represented in global climate models (GCMs) (Chang & Hong, 2011; Di Luca et al., 2012; Gensini & Mote, 2015; Lee & Hong, 2014; Mezghani et al., 2017; Wang et al., 2004). The Coordinated Regional Climate Downscaling Experiment (CORDEX) framework, sponsored by the WCRP, is a representative program that examines regional climate information from various RCMs. Quality-controlled data sets for the regional climate change scenarios were produced using CORDEX. Recently, in the East Asia (EA) branch of CORDEX (CORDEX-EA), regional climate change scenarios based on the CMIP5, and CMIP6 global climate change scenarios were produced using multi-RCMs.

In East Asia, atmospheric phenomena occur at various scales owing to the complex topography and lower boundary conditions, such as coastlines (Cha et al., 2011; Hong & Kanamitsu, 2014). Therefore, in this region, it is important to confirm small-scale phenomena that cannot be expressed in the global climate model (GCM) and assess the added value (AV) from the regional climate model (RCM). RCM is expected to provide valuable information for AV due to its relatively high resolution, enabling the capture of detailed information and heterogeneity in the lower boundary that cannot be represented at coarser resolutions. RCM can better express inland topography, land use land type and complex coastlines, and the associated regional forcing provides improved AV compared to GCM by better expressing climatic features (Rummukainen, 2016). For these regions, analyzing the current climate using the dynamically downscaled results from the RCM is essential for evaluating the systematic error in the regional climate modeling process before assessing the future climate (Giorgi & Gutowski, 2015). In East Asia, various studies have been conducted to confirm the AV of RCM using current climate-change scenarios (Ahn et al., 2018; Jin et al., 2016; Kim et al., 2021; Lee & Hong, 2014; Suh et al., 2012). Lee and Hong (2014) examined the performance of extreme weather simulations in Korea at different RCM resolutions. The RCM performed better at capturing heavy rainfall and sweltering days as the resolution increased. Ahn et al. (2018) confirmed an improved dry bias near the Korean Peninsula in the RCM compared to the forcing data. Kim et al. (2021) showed that bias-corrected RCM results are similar to the observations. Despite these results, it is not easy to clearly identify whether AV in the RCM always enhance the quality of the downscaled results. The AV of the RCM has different effects depending on various factors such as the model, variable, scale, region, and experimental configuration. Therefore, confirming where and in which elements the AV appears (Rummukainen, 2016) is essential.

Precipitation systems over the Korean Peninsula are significantly affected by migrating extratropical cyclones throughout the year. Identifying the characteristics of individual cyclones that have a significant impact on the local climate can be accomplished by determining their activity. However, using a storm track (ST) to assess the overall characteristics of the cyclones is a more efficient approach. ST is expressed as the disturbances of a specific period associated with a synoptic scale baroclinic wave and is used prominently in the East Asian regions (Chen et al., 2014; Chung et al., 1976; Whittaker & Horn, 1984). In the inland areas of East Asia, low pressure is actively generated by lee cyclogenesis on the windward side of mountain ranges, such as the Tibetan Plateau, resulting in solid ST intensity (Chung et al., 1976; Whittaker & Horn, 1984). Among the maritime regions of East Asia, cyclogenesis due to warm sea surface temperatures (SSTs) occur in the East China Sea and the Kuroshio extension region, which also affects the ST (Chen et al., 1992; Zhang et al., 2019). The cyclones formed by these factors develop toward the Aleutian Islands. Owing to these characteristics, high cyclone variability occurs in the northwestern Pacific (NWP) region.

The Northwestern Pacific storm track (NWPST) which shows maximum values in winter, is inextricably linked to the weather and climate systems of the Northern Hemisphere. Heat, moisture, and angular momentum are redistributed by ST (Mbengue & Schneider, 2018). Variations in the intensity and location of the NWPST have a distinct impact on the regional climate of East Asia (Nakamura et al., 2002; Yang et al., 2021; Zhang, Li, et al., 2014; Zhang, Qi, & Hu, 2014). Nakamura et al. (2002) confirmed that the strengthening of NWPST intensity in the late 1980s weakened the northwesterly monsoon flow from the Siberian high to the Aleutian low

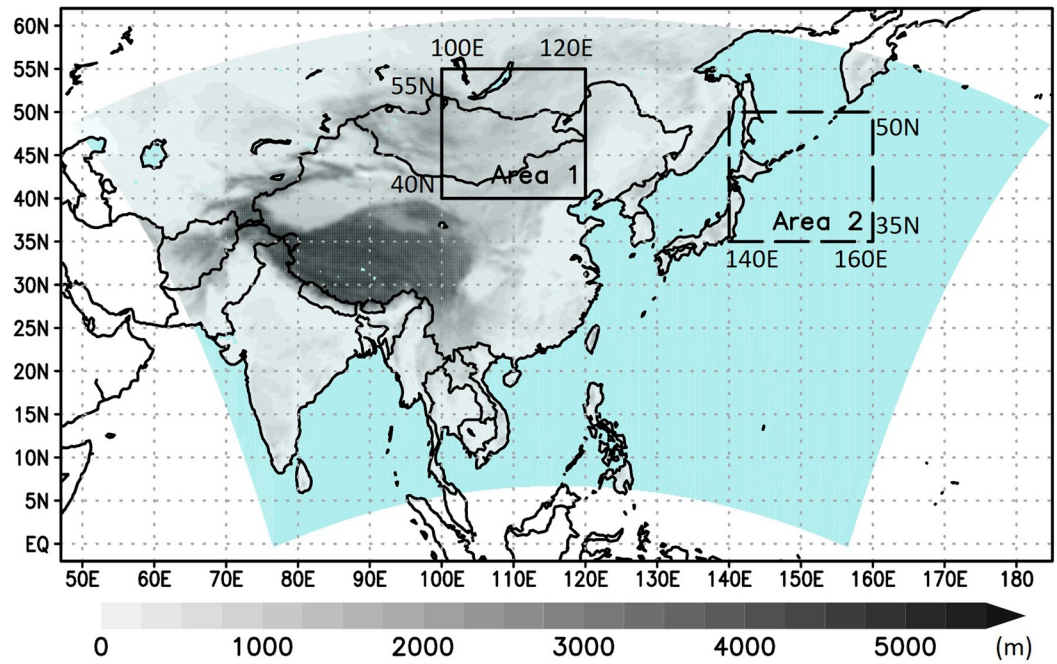

Figure 1. Regional model domain and terrain height shaded every 200 m.

region. Zhang, Li, et al. (2014) and Zhang, Qi, and Hu (2014) showed the meridional oscillation of the NWPST in the East Asian winter monsoon (EAWM) using empirical orthogonal function analysis. In addition, Yang et al. (2021) confirmed the relationship between EAWM strength and the zonal distribution of the NWPST. Enhanced cold air transport from high latitudes when the EAWM is enhanced can suppress the growth of transient eddies in the entrance region and weaken the WNPST intensity. These studies used global reanalysis data to focus on the relationship between the EAWM and NWPST. Although previous studies have focused on the relationship between the NWPST and the global climate system, there are limitations in clarifying a specific region's regional-scale climate characteristics. The characteristics of NWPST can be examined through dynamic downscaling methods using the RCM, which includes dynamic processes such as cyclogenesis, which can simulate regional-scale phenomena.

To confirm the characteristics of the local climate in winter in East Asia and the AVs in the RCM, which were not approved in the ST study using the global analysis data or GCM data, a study using the dynamically downscaled data generated through the CORDEX-EA project is conducted. In this study, the winter ST over East Asia was analyzed using the dynamic downscaling results of the RCM performed with different GCM forcings, and the effects of the AV of RCMs were addressed.

2. Data and Methods

The RCM used in this study was the Weather Research and Forecasting (WRF) Model (Skamarock & Klemp, 2008) version 3.7. The essential components of the physics package are as follows: the WRF single moment 6-class scheme (WSM6) for cloud microphysics (Hong & Lim, 2006), the rapid radiative transfer scheme for general circulation models (RRTMG) for shortwave and longwave radiation (Iacono et al., 2008), the Yonsei University (YSU) scheme for planetary boundary layers (Hong et al., 2006), and the Noah land surface model (Chen & Dudhia, 2001). The Max Planck Institute Earth System Model - Low Resolution (MPI-ESM-LR) (Giorgetta et al., 2013) from CMIP5 and United Kingdom Earth System Model 1—Low Resolution (UKESM1-0-LL) (Sellar et al., 2019) from CMIP6 provided the initial and boundary conditions for the RCM every 6 hr. The model domain for this study was centered at 34.40°N and 116.57°E, with a 25-km horizontal resolution and 33 sigma levels extending to a model top of 50 hPa, in accordance with the CORDEX East Asia Phase 2 framework (see Figure 1). Spectral nudging (Miguez-Macho et al., 2004) of the horizontal wind (U and V) was applied to retain large-scale information from the GCM during the integration of the WRF model. The large-scale structure was

employed using two-dimensional Fourier low-pass filtering with threshold wavenumbers of 9 and 6 in the x- and y-directions, respectively, which allowed the nudging of GCM information larger than approximately 1,000 km horizontally. The nudging coefficient is set to 0.0001 s^{-1}. In this study, 24 winters were analyzed from December 1981 to February 2005 for the entire model integration period of 1979–2005. The fifth-generation ECMWF's reanalysis (ERA5) was used to evaluate the simulated results. The spatial resolution of the ERA5 data was approximately 31 km, and the vertical resolution was 137 km (Hersbach et al., 2020).

The intensity of the storm track was analyzed using bandpass filtering methods for five different data sets: two GCMs, two RCM results downscaled from different GCMs, and ERA5. Bandpass filtering is a valuable method because the resultant eddy quantities reflect the intimate interaction between transient eddies and the time-mean flow (Chang, 2009; Chang et al., 2002; Hoskins & Hodges, 2019). An ST is defined as a localized maximum in the transient bandpass variance (Blackmon, 1976). Through bandpass filtering methods, it is possible to analyze the variables at every atmospheric level and investigate the three-dimensional distribution of the storm track using multi-layer information. This study used the Lanczos bandpass filtering method (Duchon, 1979) to selectively extract signals on a synoptic scale (2–7 d), including extratropical cyclones and anticyclones, and the root-mean-square of these oscillations calculated at each grid point is referred to as ST (Blackmon et al., 1984).

Denote the filtered time series at a grid point as $x(t)$, and its Hilbert transform as $\hat{x}(t)$, which lags $x(t)$ by $\pi/2$ phase, based on

$$\hat{x}(t) \approx \sum_{l=-L}^{L} x(t-l)h(l) \tag{1}$$

$$h(l) = \begin{cases} \frac{2}{\pi l}\sin^2\left(\frac{\pi l}{2}\right), & l \neq 0 \\ 0, & l = 0 \end{cases}. \tag{2}$$

Ideally $L = \infty$ in (Equation 1), but in this study $L = 28$, which provides an adequate amplitude response in the frequency domain (Barnett, 1983). After the Hilbert transform, the data for 24–30 November and 1–7 March are not available because of tapering. Hence, we only used data from the 90 d since December 1 in the following analysis.

3. Results

Figure 2 shows the average bandpass standard deviation (BPSD) of sea level pressure for December–January–February from 1982 to 2005. A high BPSD value means that cyclones pass more frequently in the area, or when cyclones pass the same number of times, cyclones with stronger intensity than low BPSD. In both cases, it means that the cyclone activity is strengthened. This cyclone activity, the storm track, plays a pioneering role in the dynamics of the mid-latitude atmosphere (Chang et al., 2002). The BPSD from ERA5 (Figure 2a) showed intense activity over continental mountainous regions and maritime regions. A high BPSD of over 450 Pa was shown over Mongolia along the Altai–Sayan Mountains to the Gobi Desert, caused by lee cyclogenesis (Chen & Lazić, 1990). The Taklamakan Desert, between the Altai Mountains and Tibet, has a relatively low BPSD of approximately 200 Pa, owing to the suppressed development of storms. In the maritime region, it has been shown that much stronger cyclone activity (BPSD over 700 Pa) than on the continent is captured over the Northwest Pacific region, which is the eastern region of Kuril Island, owing to cyclogenesis caused by warm ocean currents (Chen et al., 1992). This high BPSD is a result of the characteristics of East Asian regional storms, which gradually develop and disappear as they move to the corresponding area.

The MPI showed an overall higher cyclone activity than ERA5 over the inland area (Figure 2b), whereas the general features were similar to those of the reanalysis. For detailed features over the Altai–Sayan Mountains, the MPI simulated more robust cyclone activity with a BPSD higher than 550 Pa, including in the Taklamakan Desert region, which showed a lower BPSD in the ERA5. In the Northeast China Plain, which is the mid-area of the two analyzed PBSD cores (i.e., the Altai–Sayan and Northwest Pacific regions), the MPI showed a higher ST intensity (>400 Pa) than the reanalysis (approximately 300 Pa). However, the UKESM did not distinctly capture the inland ST intensity over the Altai–Sayan area, as shown in ERA5 (Figure 2c).

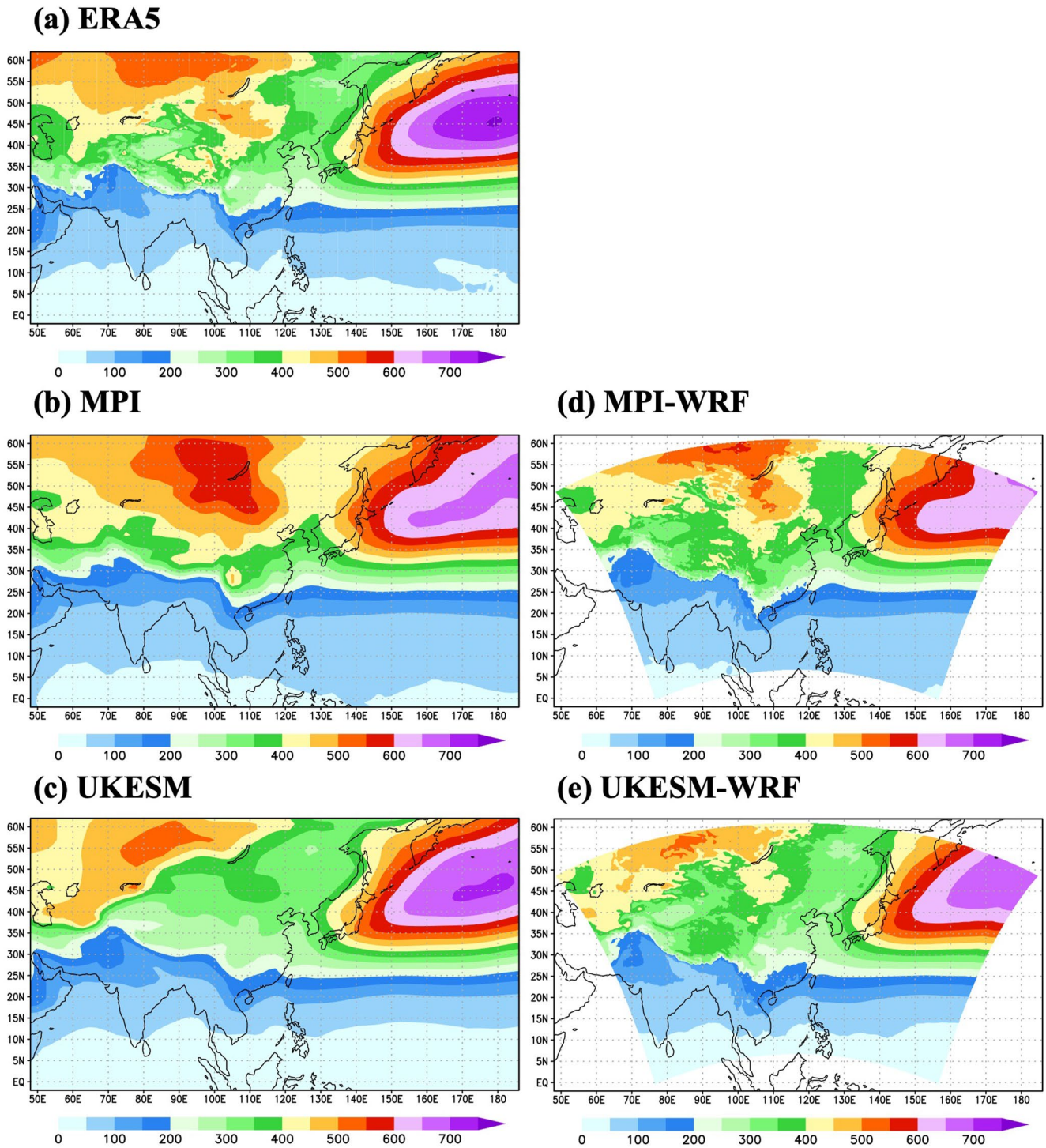

Figure 2. Averaged fields for December–January–February from 1982 to 2005 for the bandpass standard deviations of sea level pressure from the (a) ERA5 analysis, (b) MPI-ESM-LR, (c) UKESM, (d) WRF forced by MPI, and (e) WRF forced by UKESM (unit: Pa).

Figures 2d and 2e show the BPSD for the regional climate model using MPI and UKESM as the input data, respectively. Interestingly, the dynamic downscaling employed by each GCM significantly improved the bias that appeared in the inland areas. The WRF model, which used MPI global forcing data, showed a lower BPSD for sea level pressure than the GCM (Figure 2d). This offset the negative BPSD bias of approximately 150 hPa in Mongolia and its surroundings in the GCM (Figure 3a). In contrast, the opposite counterbalance appeared in

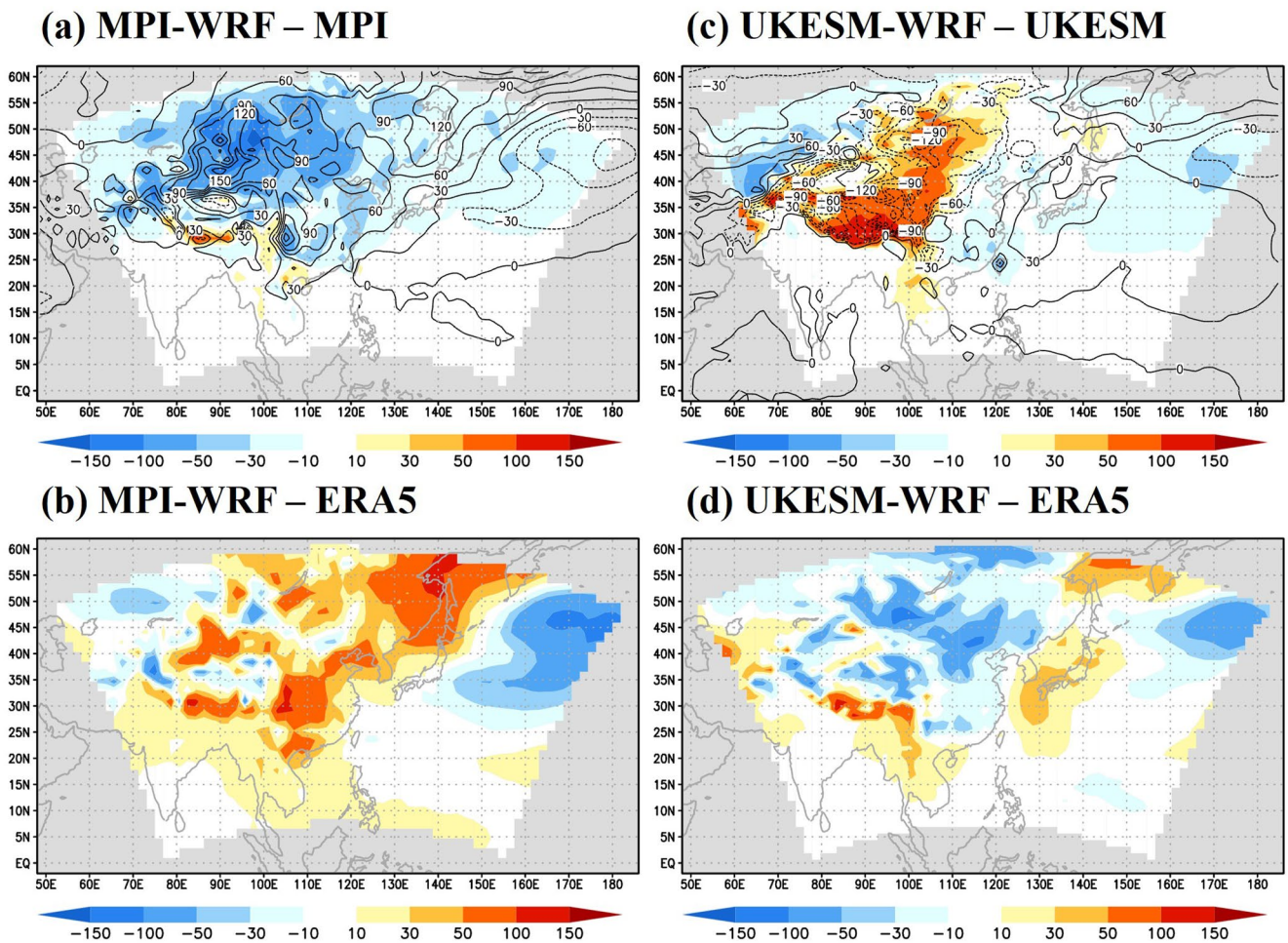

Figure 3. Bandpass standard deviation bias of WRF model regarding employed forcing GCM (shading) (a) MPI, and (c) UKESM, and the bandpass standard deviation difference between (b) WRF forced by MPI and ERA5, (d) WRF forced by UKESM and ERA5 reanalysis data. The contours in (a) and (c) denote the bandpass standard deviation bias of GCM about ERA5 reanalysis. RCM, GCM, and ERA5 data were interpolated to the resolution of the GCM with the lowest resolution using the linear interpolation method.

the WRF model using UKESM data (Figure 2e). This improved the positive bias of the GCM by approximately −120 Pa over the region from the Tibetan Plateau to the Gobi Desert (Figure 3c).

We calculate the correlation and RMSE (Root Mean Square Error) from GCMs and RCMs about ERA5 reanalysis data to confirm the improvement of bandpass statics in the dynamically downscaled RCM compared to the GCM, which is used for forcing (Table 1.). The correlation, which had a value of 0.978 in MPI, increased to 0.982 in the WRF forced by MPI, and the RMSE also decreased from 56.1 Pa in MPI to 35.6 Pa in WRF. In the case of UKESM, the correlation value, which was 0.963, increased to 0.983 in the dynamically downscaled WRF, and RMSE decreased from 44.4 Pa in UKESM to 29.2 Pa in WRF.

Table 1
Correlation and Root Mean Square Error From GCMs and RCMs

	MPI	MPI-WRF	UKESM	UKESM-WRF
Correlation	0.978	0.982	0.963	0.983
Root means square error [Pa]	56.1	35.6	44.4	29.2

Note. For each statics, bandpass statics of sea level pressure averaged over the analysis period were calculated for the area from 8°N to 56°N and from 75°E to 150°E.

The GCM has limitations in expressing a low-pressure system caused by complex terrain owing to its low resolution. The ST of Mongolia was strongly or weakly simulated, depending on the topographic information used in the GCM. The GCM data were used only as lateral boundary conditions in the RCM, and the atmospheric conditions in the inner domain were calculated using their dynamic processes. Therefore, in the RCM, a dynamic expression such as lee cyclogenesis is improved because of the high-resolution topographic data used as the lower boundary condition. Although the RCM does not entirely improve the bias of GCM (Figures 3b and 3d), this reduced the

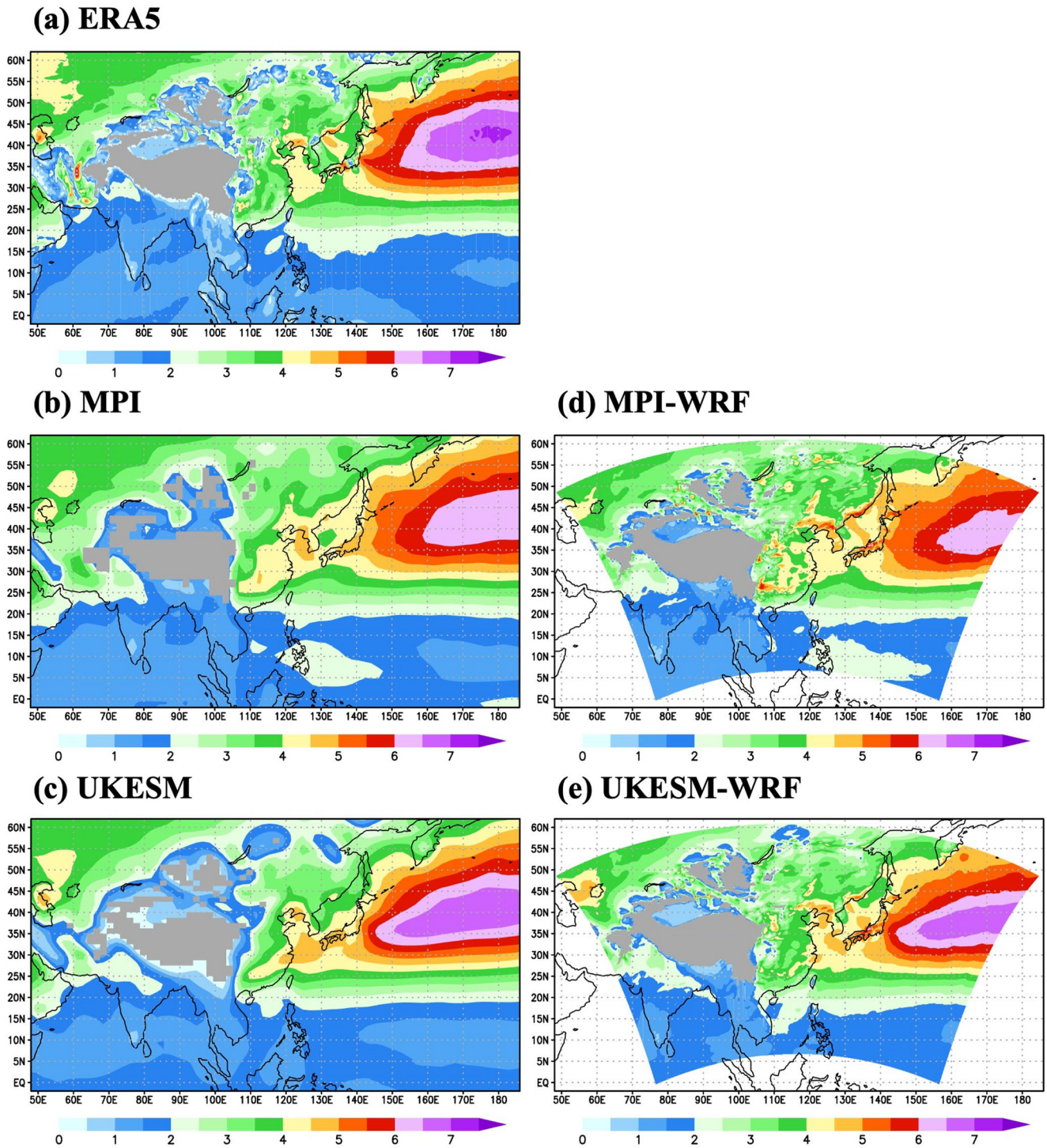

Figure 4. Same as Figure 2 but for the meridional wind at 850 hPa (unit: m s^{-1}).

bias shown by the GCM, which was close to the observations. Unlike the inland area, where dramatic changes appeared, both RCMs showed a lower BPSD (approximately 25 Pa) than the GCM, regardless of the GCM bias in the ocean. This feature appeared because the energy flux conditions at the sea surface from the global model were applied in the RCM without significant changes in the case of the ocean region.

The BPSD of the meridional wind at 850 hPa is shown in Figure 4. These figures can be used to examine the momentum and energy transport from lower to higher altitudes due to the ST in the lower troposphere. However,

small-scale phenomena expressed in ERA5 were not well resolved in the GCM, owing to its low resolution. Inland areas with complex topography, such as the Taklamakan Desert and Altai Mountains, did not express well in the BPSD values, and small-scale phenomena over inland China, such as the Sichuan Basin and Hubei Plain, were also not resolved. In contrast, in both the RCMs, characteristics similar to those of ERA5 were expressed in the corresponding regions. Small-scale phenomena on steep slopes around Tibet and inland China were decomposed and expressed. Low-pressure systems that cause heavy rainfall in East Asia, including the Korean Peninsula, are created and developed (Shin & Lee, 2015; Song et al., 2018). However, performing numerical modeling is challenging because of the unique flow structure over the steep slope of the eastern boundary of Tibet and the stagnation of the basin (Zhang, Li, et al., 2014; Zhang, Qi, & Hu, 2014).

The heat flux transmitted from low latitudes to high latitudes in the Northwestern Pacific in winter dramatically affects the local climate (Nakamura et al., 2002). The meridional eddy heat flux is expressed as the product of the perturbation term of temperature and the perturbation term of north-south wind at a specific level. Figure 5 shows the BPSD of the meridional eddy heat flux distribution, a typical feature of the Northwest Pacific region during the winter season. In ERA5, the BPSD of the heat flux core appeared in the Northwest Pacific region, with a central value of approximately 15 K m s^{-1}. In the MPI, the central value is 12 K m s^{-1}, which is lower than that of ERA5, and in the UKESM, it appears similar to that of ERA5. In the WRF model, the heat flux cores over this region are similar to the GCM forcing employed. Additionally, in ERA5, there was a high eddy heat flux region along the northern coastal part of the Korean Peninsula, such as the Gulf of Pohai and Peter Great Bay. These two cores were simulated as one in both the MPI and UKESM results. However, in the WRF model, the small-scale feature of heat flux over the coastal region was represented. In particular, the high BPSD of the heat flux band from the Peter Great Bay to Japan is well expressed. The characteristics of small-scale bandpass statics in coastal areas clearly expressed in RCM are because the coastline is clearly defined at high resolution. Depending on whether the lower surface type is determined as land or ocean, the surface energy balance in the region is distinctly different. In the case of RCM, which has a relatively high resolution, the energy flux transferred from the land or ocean to the atmosphere in the coastal area can be expressed close to reality.

The time series of the BPSD of the sea level pressure is shown in Figure 6. To confirm the AV of the RCM, we established the analyzed regions marked in Figure 1 for the land and ocean areas. The land area is mainly composed of the Altai Mountains region, where AV is evident, and the ocean area is the Northwest Pacific region, including the Kuril Islands. The ocean area is located west of the site where the maximum BPSD statistics appear, but it is configured to make the area less affected by the buffer zone. The annual variation in the BPSD of sea level pressure from the RCM shows similar behavior to that of the GCM. As shown in Figures 2 and 3, which are analyzed as the average values for the entire period, MPI overestimates the bandpass filtered value, and UKESM underestimates it, respectively, compared to the ERA5 reanalysis data. The two WRF models, which were forced by MPI and UKESM data, improved the bias for bandpass filtered value despite having opposite directions overall. The WRF model, which employed UKESM, shows a bias of 36 Pa compared to UKESM, and that employed MPI represented a bias of −62 Pa. This value appeared to be constant over the entire period. In the case of a specific year in which the bias of the GCMs was expressed differently from the common years, the AV from the RCMs increased the GCMs' bias due to the climate model's characteristics that cannot modify the actual atmosphere state. The bandpass statistics from both GCMs showed relatively similar ERA5 values for the ocean. The simulated bandpass-filtered standard deviations of sea-level pressure values in the RCM were −11 Pa for UKESM and −20 Pa for MPI, which were lower than those for land.

4. Summary

This study provides evidence for the impact of the RCM AV on dynamical downscaling outcomes in the East Asian region. Two different GCMs (MPI for CMIP5 and UKESM for CMIP6) were compared by forcing the WRF model. The bandpass filtering method was used to separate the synoptic scale (2–7 d) to represent the storm track. The spectral nudging method was applied to all layers of the WRF data, except the planetary boundary layer, to ensure risk control during decades of integration. The RCM bandpass statistics in the middle- and upper-troposphere storm tracks were similar to those of the GCM (not shown). As a result, this study concentrates on surface and lower tropospheric storm tracks.

The AV of the RCM in East Asia differs depending on the region. The use of RCM AV in this study helped to reduce the bias of the GCM over inland high-altitude regions, such as the Tibetan Plateau or Mongolia, bringing

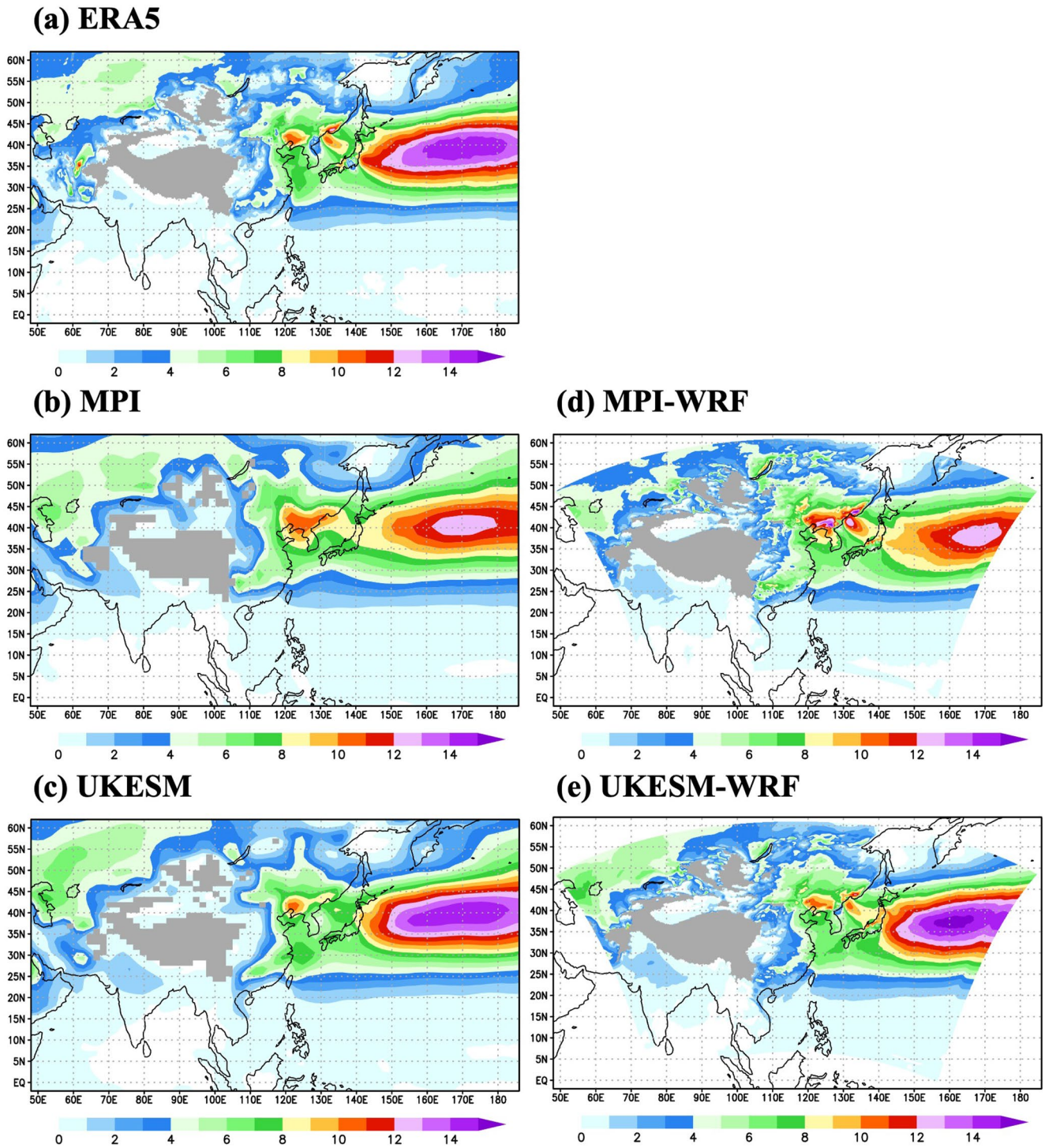

Figure 5. Same as Figure 2 but for the meridional eddy heat flux at 850 hPa (unit: km s^{-1}).

the results closer to the reanalysis. These characteristics appear to result from the dynamic balance within the RCM due to the high-resolution lower boundary information, such as topography and land use land cover. Owing to the high-resolution surface information, dynamic phenomena, such as lee cyclogenesis, are well simulated in the RCM. In the eastern flank of the Tibetan Plateau and the coastal region, the characteristics of the AV due to the increase in horizontal resolution were well confirmed. Small-scale phenomena that are not expressed in the GCM are well represented. In the maritime region, the ST of the RCM was similar to that of the GCM. In

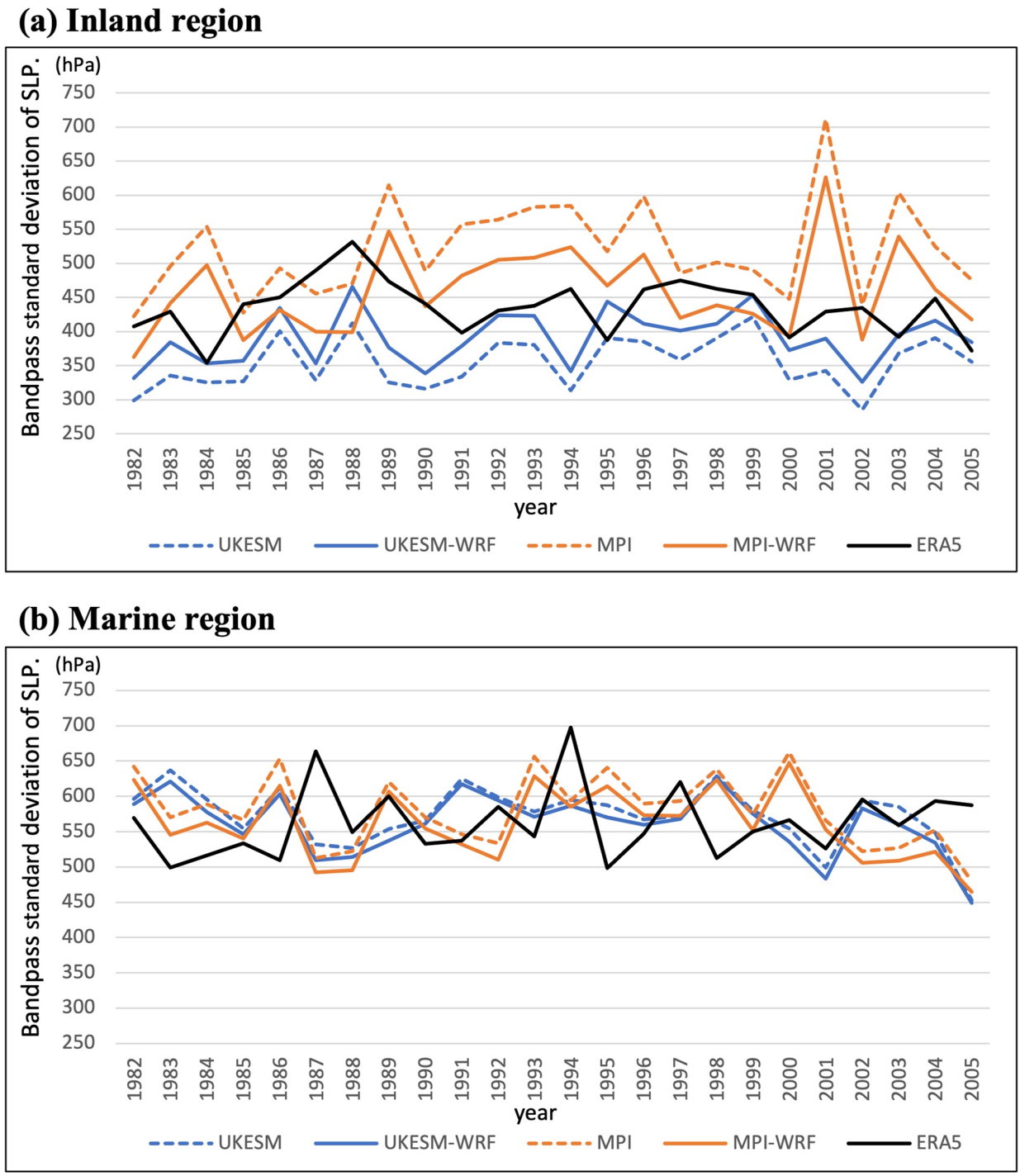

Figure 6. Time series of bandpass standard deviations of sea level pressure which are presented for the (a) inland region marked as a solid box and (b) marine region marked as a dashed box in Figure 1. In each figure, the blue dashed line is the value of UKESM, the blue solid line is the value of the WRF forced by UKESM, the orange dashed line is the value of MPI, the orange solid line is the value of the WRF forced by MPI, and the black solid line represents the value of ERA5.

the numerical model, the atmosphere over the ocean is sensitive to lower boundary conditions, such as surface temperature, as in nature (Kim & Hong, 2010). Unlike the land, which requires dynamic rebalancing, the lower atmosphere of the RCM is greatly affected by the lower boundary conditions of the GCM. According to previous studies, when high-resolution SST data is employed, the model simulates oceanic cyclogenesis well (Small et al., 2014; Zhang et al., 2019). As ocean fronts are clearly expressed in high-resolution SST data, the transient

eddy heat and moisture fluxes in the lower layer are also well expressed, and these effects influence the troposphere beyond the boundary layer. In the Northwest Pacific region, the importance of high-resolution SST is even more remarkable because there is a warm current that expresses oceanic eddies, such as the Kuroshio Current. Explosive cyclones that develop in the northwestern Pacific region during winter (Roebber, 1984; Sanders & Gyakum, 1980) are closely related to strong winds and extreme weather in East Asia (Kang et al., 2020). Therefore, it is important to use accurate and high-resolution SST data as input for the model. It is necessary to increase the resolution and elaborate on the lower boundary conditions to improve the AV of the RCM. In inland regions, the refinement of information, such as topography, soil, and vegetation is required. In the case of climate models older than a decade, a reliable scenario should be produced if the model considers surface information changes. Maritime areas require reliable ocean information. Unlike past reproduction experiments that can utilize high-resolution SST data, future climate change scenario production, which makes it impossible to use analysis data, can improve the performance of oceanic cyclogenesis simulations through an atmospheric-marine coupled model. The interactions between the ocean and atmosphere in the coupled model provide desirable information on the formation and development of cyclones.

Data Availability Statement

The model simulation data used in this study are available upon reasonable request from the authors and will be publicly available at https://esg-dn1.nsc.liu.se/search/cordex/ in the future. The ERA5 data were downloaded from Copernicus Climate Change Service (C3S) Climate Data Store (CDS) (Copernicus Climate Change Service & Climate Data Store, 2023) https://cds.climate.copernicus.eu/cdsapp#!/dataset/reanalysis-era5-complete?tab=overview. The MPI-ESM-LR data can be downloaded from World Data Center for Climate (WDCC) at DKRZ (Jungclaus et al., 2013) https://esgf-node.llnl.gov/search/cmip5/ and UKESM1-0-LL data can be downloaded from Earth System Grid Federation (Tang et al., 2019) https://esgf-node.llnl.gov/search/cmip6/.

Acknowledgments
This study was funded by the Korea Meteorological Administration Research and Development Program (Grant KMI2020-01411). This work was also supported by a research grant from the Kongju National University in 2021.

References

Ahn, J. B., Choi, Y. W., & Jo, S. (2018). Evaluation of reproduced precipitation by WRF in the Region of CORDEX-East Asia phase 2. *Atmosphere*, *28*(1), 85–97. https://doi.org/10.14191/Atmos.2018.28.1.085

Barnett, T. P. (1983). Interaction of the monsoon and Pacific trade wind system at interannual time scales part I: The equatorial zone. *Monthly Weather Review*, *111*(4), 756–773. https://doi.org/10.1175/1520-0493(1983)111<0756:iotmap>2.0.co;2

Blackmon, M. L. (1976). A climatological spectral study of the 500 mb geopotential height of the Northern Hemisphere. *Journal of the Atmospheric Sciences*, *33*(8), 1607–1623. https://doi.org/10.1175/1520-0469(1976)033<1607:ACSSOT>2.0.CO;2

Blackmon, M. L., Lee, Y. H., Wallace, J. M., & Hsu, H. H. (1984). Time variation of 500 mb height fluctuations with long, intermediate and short time scales as deduced from lag-correlation statistics. *Journal of the Atmospheric Sciences*, *41*(6), 981–991. https://doi.org/10.1175/1520-0469(1984)041<0981:tvomhf>2.0.co;2

Cha, D. H., Jin, C. S., Lee, D. K., & Kuo, Y. H. (2011). Impact of intermittent spectral nudging on regional climate simulation using Weather Research and Forecasting model. *Journal of Geophysical Research*, *116*(D10), D10103. https://doi.org/10.1029/2010JD015069

Chang, E. C., & Hong, S. Y. (2011). Projected climate change scenario over East Asia by a regional spectral model. *Journal of the Korean Earth Science Society*, *32*(7), 770–783. https://doi.org/10.5467/JKESS.2011.32.7.770

Chang, E. K. (2009). Are band-pass variance statistics useful measures of storm track activity? Re-examining storm track variability associated with the NAO using multiple storm track measures. *Climate Dynamics*, *33*(2–3), 277–296. https://doi.org/10.1007/s00382-009-0532-9

Chang, E. K., Lee, S., & Swanson, K. L. (2002). Storm track dynamics. *Journal of Climate*, *15*(16), 2163–2183. https://doi.org/10.1175/1520-0442(2002)015<02163:STD>2.0.CO;2

Chen, C., Beardsley, R. C., & Limeburner, R. (1992). The structure of the Kuroshio southwest of Kyushu: Velocity, transport and potential vorticity fields. *Deep-Sea Research, Part A: Oceanographic Research Papers*, *39*(2), 245–268. https://doi.org/10.1016/0198-0149(92)90108-6

Chen, F., & Dudhia, J. (2001). Coupling an advanced land surface–hydrology model with the Penn State–NCAR MM5 modeling system. Part I: Model implementation and sensitivity. *Monthly Weather Review*, *129*(4), 569–585. https://doi.org/10.1175/1520-0493(2001)129<0569:CAALSH>2.0.CO;2

Chen, L., Tan, B., Kvamstø, N. G., & Johannessen, O. M. (2014). Wintertime cyclone/anticyclone activity over China and its relation to upper tropospheric jets. *Tellus A: Dynamic Meteorology and Oceanography*, *66*(1), 21889. https://doi.org/10.3402/tellusa.v66.21889

Chen, S. J., & Lazić, L. (1990). Numerical case study of the Altai-Sayan lee cyclogenesis over east Asia. *Meteorology and Atmospheric Physics*, *42*(3), 221–229. https://doi.org/10.1007/BF01314826

Chung, Y. S., Hage, K. D., & Reinelt, E. R. (1976). On lee cyclogenesis and airflow in the Canadian Rocky Mountains and the East Asian Mountains. *Monthly Weather Review*, *104*(7), 879–891. https://doi.org/10.1175/1520-0493(1976)104<0879:OLCAAI>2.0.CO;2

Copernicus Climate Change Service & Climate Data Store. (2023). ERA5 hourly data from 1982 to 2005 [Dataset]. Copernicus Climate Change Service (C3S) Climate Data Store (CDS). Retrieved from https://cds.climate.copernicus.eu/cdsapp#!/dataset/reanalysis-era5-complete?tab=overview

Di Luca, A., de Elía, R., & Laprise, R. (2012). Potential for added value in precipitation simulated by high-resolution nested regional climate models and observations. *Climate Dynamics*, *38*(5–6), 1229–1247. https://doi.org/10.1007/s00382-011-1068-3

Duchon, C. E. (1979). Lanczos filtering in one and two dimensions. *Journal of Applied Meteorology and Climatology*, *18*(8), 1016–1022. https://doi.org/10.1175/1520-0450(1979)018<1016:LFIOAT>2.0.CO;2

Eyring, V., Bony, S., Meehl, G. A., Senior, C. A., Stevens, B., Stouffer, R. J., & Taylor, K. E. (2016). Overview of the Coupled Model Intercomparison Project Phase 6 (CMIP6) experimental design and organization. *Geoscientific Model Development*, *9*(5), 1937–1958. https://doi.org/10.5194/gmd-9-1937-2016

Gensini, V. A., & Mote, T. L. (2015). Downscaled estimates of late 21st century severe weather from CCSM3. *Climatic Change*, *129*(1), 307–321. https://doi.org/10.1007/s10584-014-1305-z

Giorgetta, M. A., Jungclaus, J., Reick, C. H., Legutke, S., Bader, J., Böttinger, M., et al. (2013). Climate and carbon cycle changes from 1850 to 2100 in MPI-ESM simulations for the Coupled Model Intercomparison Project phase 5. *Journal of Advances in Modeling Earth Systems*, *5*(3), 572–597. https://doi.org/10.1002/jame.20038

Giorgi, F., & Gutowski, W. J., Jr. (2015). Regional dynamical downscaling and the CORDEX initiative. *Annual Review of Environment and Resources*, *40*(1), 467–490. https://doi.org/10.1146/annurev-environ-102014-021217

Hersbach, H., Bell, B., Berrisford, P., Hirahara, S., Horányi, A., Muñoz-Sabater, J., et al. (2020). The ERA5 global reanalysis. *Quarterly Journal of the Royal Meteorological Society*, *146*(730), 1999–2049. https://doi.org/10.1002/qj.3803

Hong, S. Y., & Kanamitsu, M. (2014). Dynamical downscaling: Fundamental issues from an NWP point of view and recommendations. *Asia-Pacific Journal of Atmospheric Sciences*, *50*(1), 83–104. https://doi.org/10.1007/s13143-014-0029-2

Hong, S. Y., & Lim, J. O. J. (2006). The WRF single-moment 6-class microphysics scheme (WSM6). *Asia-Pacific Journal of Atmospheric Sciences*, *42*(2), 129–151. https://doi.org/10.1007/s13143-016-0011-z

Hong, S. Y., Noh, Y., & Dudhia, J. (2006). A new vertical diffusion package with an explicit treatment of entrainment processes. *Monthly Weather Review*, *134*(9), 2318–2341. https://doi.org/10.1175/MWR3199.1

Hoskins, B. J., & Hodges, K. I. (2019). The annual cycle of Northern Hemisphere storm tracks. Part I: Seasons. *Journal of Climate*, *32*(6), 1743–1760. https://doi.org/10.1175/JCLI-D-18-0061.1

Hsiang, S., Kopp, R., Jina, A., Rising, J., Delgado, M., Mohan, S., et al. (2017). Estimating economic damage from climate change in the United States. *Science*, *356*(6345), 1362–1369. https://doi.org/10.1126/science.aal4369

Iacono, M. J., Delamere, J. S., Mlawer, E. J., Shephard, M. W., Clough, S. A., & Collins, W. D. (2008). Radiative forcing by long-lived greenhouse gases: Calculations with the AER radiative transfer models. *Journal of Geophysical Research*, *113*(D13), D13103. https://doi.org/10.1029/2008JD009944

Jin, C. S., Cha, D. H., Lee, D. K., Suh, M. S., Hong, S. Y., Kang, H. S., & Ho, C. H. (2016). Evaluation of climatological tropical cyclone activity over the western North Pacific in the CORDEX-East Asia multi-RCM simulations. *Climate Dynamics*, *47*(3), 765–778. https://doi.org/10.1007/s00382-015-2874-8

Jungclaus, J. H., & Coauthors (2013). CMIP5 simulations of the Max Planck Institute for Meteorology (MPI-M) based on the MPI-ESM-LR model: The decadal experiments, served by ESGF [Dataset]. World Data Center for Climate (WDCC) at DKRZ. https://doi.org/10.1594/WDCC/CMIP5.MXELDEC

Kang, J. M., Lee, J., Son, S. W., Kim, J., & Chen, D. (2020). The rapid intensification of East Asian cyclones around the Korean Peninsula and their surface impacts. *Journal of Geophysical Research: Atmospheres*, *125*(2), e2019JD031632. https://doi.org/10.1029/2019JD031632

Kim, E. J., & Hong, S. Y. (2010). Impact of air-sea interaction on East Asian summer monsoon climate in WRF. *Journal of Geophysical Research*, *115*(D19), D15115. https://doi.org/10.1029/2010JD013892

Kim, G., Cha, D. H., Park, C., Jin, C. S., Lee, D. K., Suh, M. S., et al. (2021). Evaluation and projection of regional climate over East Asia in CORDEX-East Asia Phase I experiment. *Asia-Pacific Journal of Atmospheric Sciences*, *57*(1), 119–134. https://doi.org/10.1007/s13143-021-00224-6

Lee, J. W., & Hong, S. Y. (2014). Potential for added value to downscaled climate extremes over Korea by increased resolution of a regional climate model. *Theoretical and Applied Climatology*, *117*(3), 667–677. https://doi.org/10.1007/s00704-013-1021-1

Mbengue, C., & Schneider, T. (2018). Linking Hadley circulation and storm tracks in a conceptual model of the atmospheric energy balance. *Journal of the Atmospheric Sciences*, *75*(3), 841–856. https://doi.org/10.1126/science.aba9757

Meehl, G. A., Boer, G. J., Covey, C., Latif, M., & Stouffer, R. J. (1997). Intercomparison makes for a better climate model. *Eos, Transactions American Geophysical Union*, *78*(41), 445–451. https://doi.org/10.1029/97EO00276

Mezghani, A., Dobler, A., Haugen, J. E., Benestad, R. E., Parding, K. M., Piniewski, M., et al. (2017). CHASE-PL climate projection dataset over Poland–bias adjustment of EURO-CORDEX simulations. *Earth System Science Data*, *9*(2), 905–925. https://doi.org/10.5194/essd-9-905-2017

Miguez-Macho, G., Stenchikov, G. L., & Robock, A. (2004). Spectral nudging to eliminate the effects of domain position and geometry in regional climate model simulations. *Journal of Geophysical Research*, *109*(D13), D13104. https://doi.org/10.1029/2003jd004495

Moss, R. H., Edmonds, J. A., Hibbard, K. A., Manning, M. R., Rose, S. K., Van Vuuren, D. P., et al. (2010). The next generation of scenarios for climate change research and assessment. *Nature*, *463*(7282), 747–756. https://doi.org/10.1038/nature08823

Nakamura, H., Izumi, T., & Sampe, T. (2002). Interannual and decadal modulations recently observed in the Pacific storm track activity and East Asian winter monsoon. *Journal of Climate*, *15*(14), 1855–1874. https://doi.org/10.1175/1520-0442(2002)015<1855:IADMRO>2.0.CO;2

O'Neill, S., & O'Driscoll, L. (2015). Metabolic syndrome: A closer look at the growing epidemic and its associated pathologies. *Obesity Reviews*, *16*(1), 1–12. https://doi.org/10.1111/obr.12229

Roebber, P. J. (1984). Statistical analysis and updated climatology of explosive cyclones. *Monthly Weather Review*, *112*(8), 1577–1589. https://doi.org/10.1175/1520-0493(1984)112<1577:SAAUCO>2.0.CO;2

Rummukainen, M. (2016). Added value in regional climate modeling. *Wiley Interdisciplinary Reviews: Climate Change*, *7*(1), 145–159. https://doi.org/10.1186/s40562-022-00247-6

Sanders, F., & Gyakum, J. R. (1980). Synoptic-dynamic climatology of the "bomb". *Monthly Weather Review*, *108*(10), 1589–1606. https://doi.org/10.1175/1520-0493(1980)108<1589:SDCOT>2.0.CO;2

Sellar, A. A., Jones, C. G., Mulcahy, J. P., Tang, Y., Yool, A., Wiltshire, A., et al. (2019). UKESM1: Description and evaluation of the UK Earth system model. *Journal of Advances in Modeling Earth Systems*, *11*(12), 4513–4558. https://doi.org/10.1029/2019MS001739

Shin, U., & Lee, T. Y. (2015). Origin, evolution and structure of meso-α-scale lows associated with cloud clusters and heavy rainfall over the Korean peninsula. *Asia-Pacific Journal of Atmospheric Sciences*, *51*(3), 259–274. https://doi.org/10.1007/s13143-015-0076-3

Skamarock, W. C., & Klemp, J. B. (2008). A time-split nonhydrostatic atmospheric model for weather research and forecasting applications. *Journal of Computational Physics*, *227*(7), 3465–3485. https://doi.org/10.1016/j.jcp.2007.01.037

Small, R. J., Tomas, R. A., & Bryan, F. O. (2014). Storm track response to ocean fronts in a global high-resolution climate model. *Climate Dynamics*, *43*(3), 805–828. https://doi.org/10.1007/s00382-013-1980-9

Song, I. S., Byun, U. Y., Hong, J., & Park, S. H. (2018). Domain-size and top-height dependence in regional predictions for the Northeast Asia in spring. *Atmospheric Science Letters*, *19*(1), e799. https://doi.org/10.1002/asl.799

Suh, M. S., Oh, S. G., Lee, D. K., Cha, D. H., Choi, S. J., Jin, C. S., & Hong, S. Y. (2012). Development of new ensemble methods based on the performance skills of regional climate models over South Korea. *Journal of Climate*, *25*(20), 7067–7082. https://doi.org/10.1175/JCLI-D-11-00457.1

Tang, Y., & Coauthors (2019). MOHC UKESM1.0-LL model output prepared for CMIP6 CMIP historical [Dataset]. Earth System Grid Federation. https://doi.org/10.22033/ESGF/CMIP6.6113

Taylor, K. E., Stouffer, R. J., & Meehl, G. A. (2012). An overview of CMIP5 and the experiment design. *Bulletin of the American Meteorological Society*, *93*(4), 485–498. https://doi.org/10.1175/BAMS-D-11-00094.1

Wang, Y., Leung, L. R., McGregor, J. L., Lee, D. K., Wang, W. C., Ding, Y., & Kimura, F. (2004). Regional climate modeling: Progress, challenges, and prospects. *Journal of the Meteorological Society of Japan. Ser. II*, *82*(6), 1599–1628. https://doi.org/10.2151/jmsj.82.1599

Whittaker, L. M., & Horn, L. H. (1984). Northern Hemisphere extratropical cyclone activity for four mid-season months. *Journal of Climatology*, *4*(3), 297–310. https://doi.org/10.1002/joc.3370040307

Yang, M., Li, C., Li, X., Tan, Y., Chen, X., & Zhang, C. (2021). Interdecadal change in the relationship between the winter North Pacific storm track and the East Asian winter monsoon. *Journal of Climate*, *34*(8), 3171–3187. https://doi.org/10.1175/JCLI-D-20-0372.1

Zhang, M., Qi, Y., & Hu, X. M. (2014). Impact of East Asian winter monsoon on the P acific storm track. *Meteorological Applications*, *21*(4), 873–878. https://doi.org/10.1002/met.1423

Zhang, P., Li, G., Fu, X., Liu, Y., & Li, L. (2014). Clustering of Tibetan Plateau vortices by 10–30-day intraseasonal oscillation. *Monthly Weather Review*, *142*(1), 290–300. https://doi.org/10.1175/MWR-D-13-00137.1

Zhang, X., Ma, X., & Wu, L. (2019). Effect of mesoscale oceanic eddies on extratropical cyclogenesis: A tracking approach. *Journal of Geophysical Research: Atmospheres*, *124*(12), 6411–6422. https://doi.org/10.1029/2019JD030595